npj | flexible electronics

Article

Published in partnership with Nanjing Tech University

https://doi.org/10.1038/s41528-025-00415-6

Tactile near-sensor computing systems incorporating hourglass-shaped microstructured capacitive sensors for bio-realistic energy efficiency

Jae-Yeong Cho[1], Seong Eun Kim[2], Chang-Jae Beak[1], Jihwan Lee[1], Wonjeong Suh[3], Bo-Yeon Lee[3] ✉ & Sin-Hyung Lee[1] ✉

Bio-inspired near-sensor computing, which integrates sensing and processing functions, presents a promising strategy to enhance efficiency and reduce latency in such applications. Here, we introduce tactile sensory nerve systems with biologically realistic energy efficiency, utilizing starfish-inspired capacitive pressure sensors integrated with flexible memristors. These starfish-inspired sensors, with their high aspect ratio (~3) and stress-focusing, hourglass-shaped dielectric microstructures, enable highly sensitive tactile detection across a broad pressure range, effectively mimicking the properties of human skin. Artificial tactile sensory nerves, which integrate the capacitive sensor with a flexible memristor exhibiting synaptic plasticity, function reliably as energy-efficient near-sensor computing systems by bio-realistically transducing mechanical stimuli into transient electrical signals. The developed system operates as both an artificial nociceptor and a tactile near-sensor computing unit, with energy consumption approaching biological levels at approximately 140 pJ and 2.2 fJ, respectively. This neuro-inspired localized computing strategy offers a physical platform for advanced smart user interface applications.

In the era of ubiquitous computing, the volume of data to be collected and processed in user-interface applications, such as portable and wearable electronics, is rapidly increasing[1–3]. Near-sensor computing presents an attractive solution by integrating sensor data acquisition with signal processing and computation, thereby improving efficiency and reducing latency[4,5]. This architecture emulates the biological sensory nervous system, where sensory receptors and neurons collaborate to enable efficient signal detection and processing, forming an integrated system of computing devices and sensors. To develop artificial sensory nerves for practical user-interface applications, it is essential to create energy-efficient bio-inspired systems near biological levels[4,6]. This requires effective integration design of sensing and neuronal devices to enable advanced sensing and processing capabilities. While several approaches have been explored for practical neuromorphic systems, most studies on near-sensor computing have primarily focused on neuronal devices, such as synaptic transistors[7,8] and memristors[9–11], rather than sensing components. This narrow focus limits the neuromorphic performance of the overall computing system, posing a significant barrier to the development of energy-efficient systems.

Tactile stimuli play a crucial role in human-machine interfaces, providing essential external information such as health status, safety, and user movement[12,13]. Various electronic skin systems incorporating memristors or synaptic transistors integrated with pressure sensors have been developed as artificial nociceptors, capable of instantly detecting harmful stimuli and locally pre-processing analog tactile signals[14–16]. Most research on tactile sensor-memristor systems has employed simplified approaches using resistive sensors due to their compatibility with the resistive switching characteristics of neuronal devices. However, these sensors convert tactile signals into voltage pulses applied to neuronal elements under DC voltage conditions, leading to increased energy consumption proportional to the duration of the stimulus, which is not analogous to biological processes. Although piezoelectric sensing components integrated with artificial neurons have been reported to enable low-energy sensory operations, this

[1]School of Advanced Fusion Studies, Department of Intelligent Semiconductor Engineering, University of Seoul, 163 Seoulsiripdaero, Dongdaemun-gu, Seoul, 02504, Republic of Korea. [2]School of Electronic and Electrical Engineering, Kyungpook National University, 80 Daehak-ro, Buk-gu, Daegu, 702-701, Republic of Korea. [3]Department of Bionic Machinery, Research Institute of AI Robotics, Korea Institute of Machinery and Materials, Daejeon, Republic of Korea.
✉e-mail: bylee@kimm.re.kr; sinhlee@uos.ac.kr

architecture is constrained to a simple cognitive process due to the instability of neuronal conductance governed solely by external stimuli. Therefore, developing tactile sensors suitable for bio-realistic near-sensor computing is critical, along with establishing a comprehensive strategy that includes customized designs for high energy efficiency from the device to system level.

Here, we demonstrate a highly energy-efficient tactile sensory nervous system utilizing starfish-inspired capacitive pressure sensors and flexible memristors, enabling practical near-sensor computing applications (Fig. 1a and 1b). We develop a capacitive sensor with high sensitivity across a wide range by introducing a high-aspect-ratio microstructured dielectric layer inspired by the hourglass-shaped surface of the starfish, *Astropecten polyacanthus*, functioning as a tactile sensory receptor. The sensors effectively detect a wide pressure range, akin to human skin[17], from subtle pressures below 1 kPa to deep pressures up to 100 kPa, achieving high sensitivity with a peak value of 2.81 kPa^{-1} in the low-pressure range. Building on the promising sensing properties of the capacitive tactile receptor, artificial sensory nerves, comprising this sensor and a flexible memristor with stable short- and long-term plasticity (STP and LTP), reliably function as highly energy-efficient near-sensor computing systems. Due to the high sensitivity of the sensory receptors across a wide range, the magnitude and width of the electric pulses in the memristors are effectively modulated by the amplitude of the external pressure signal. Additionally, the capacitive receptor within the tactile sensory nervous system transduces mechanical stimuli into transient electrical spikes during its charging process, enabling neuronal operations with energy consumption approaching biological levels (Fig. 1a). The proposed tactile sensory nerves demonstrate significant potential for practical edge computing applications, capable of responding to both large and delicate mechanical stimuli. These include artificial nociceptors and smart fingerprint processing systems, as shown in Fig. 1b.

Results

Capacitive sensors with high sensitivity to wide pressure range

In developing a capacitive pressure sensor capable of functioning as a tactile sensory receptor, it is crucial to achieve high sensitivity across a wide stimulus range. Introducing microstructures onto a dielectric layer sandwiched between electrodes is a promising and straightforward strategy for enhancing the sensitivity of a capacitive pressure sensor[18,19]. The microstructured dielectric layer enhances the compressibility and viscoelasticity of pressure sensors, and these improvements in sensor sensitivity depend on the geometry of the microstructures, including their aspect ratio. The aspect ratio of the microstructures is a key determinant of the detection range in microstructured pressure sensors[20,21]. To fabricate a high-aspect-ratio microstructured dielectric film conducive to mechanical deformation, we replicated the surface of the starfish, which is characterized by hourglass-shaped protrusions, using the elastomeric polymer polydimethylsiloxane (PDMS) (Fig. 1a). A PDMS mold cast from the starfish's protruding surface structures served as the template for the dielectric film (Supplementary Fig. 1). The microstructured film, molded from the template, exhibited hourglass-shaped protrusions with an aspect ratio of approximately 3,

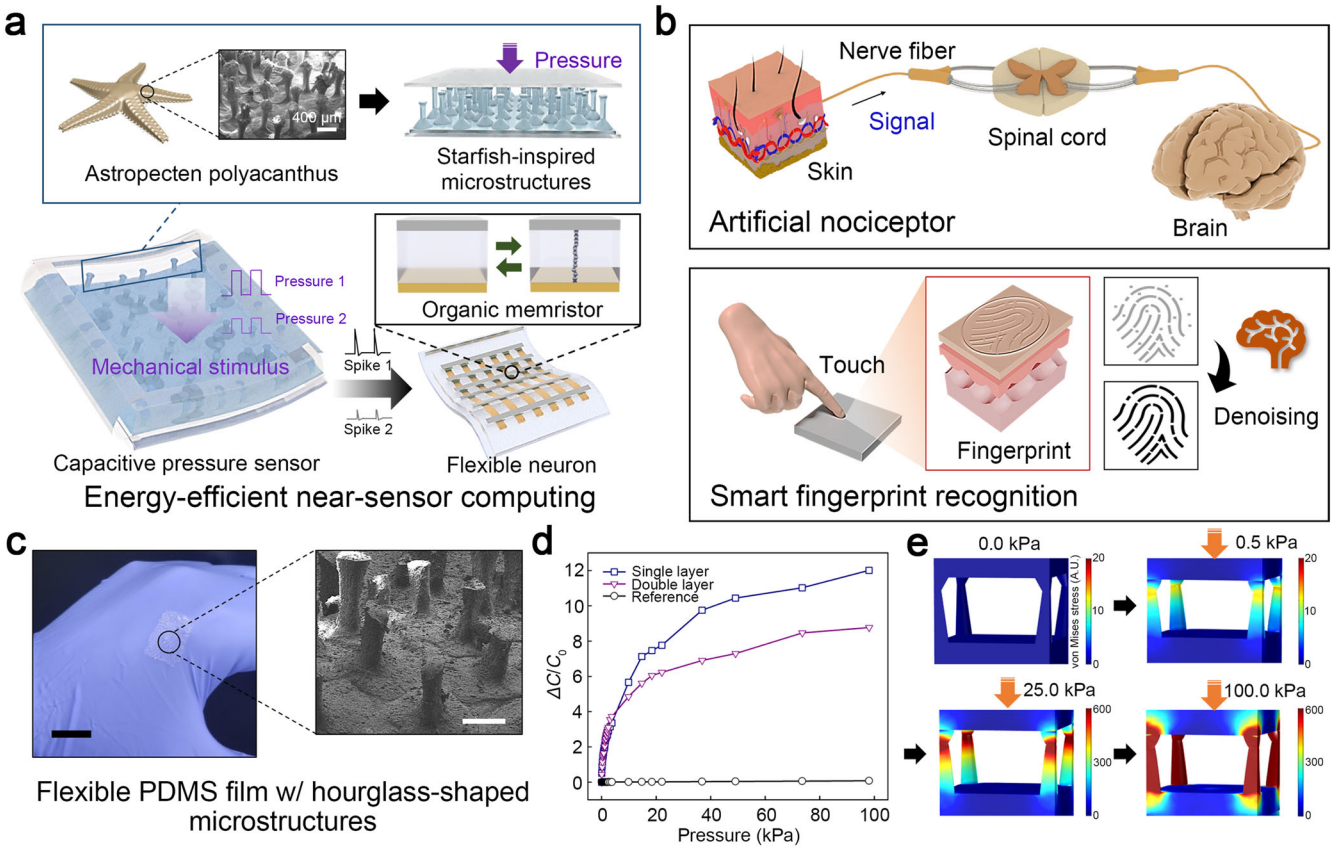

Fig. 1 | Hourglass-shaped microstructured capacitive sensors as tactile sensory receptors for energy-efficient near-sensor computing. a Conceptual illustration of a pressure sensor with a microstructured dielectric layer, mimicking the surface of the starfish, Astropecten polyacanthus, designed for energy-efficient near-sensor computing. **b** Applications of tactile near-sensor computing with high energy efficiency. **c** A flexible dielectric layer featuring hourglass-shaped microstructures. Polydimethylsiloxane (PDMS) was used as the dielectric material. Scale bar, 1.5 cm. The inset image shows the microstructures on the film, observed using field emission scanning electron microscopy. Scale bar, 400 μm. **d** Normalized capacitive responses of pressure sensors with single and double dielectric layers incorporating hourglass-shaped microstructures, and a conventional flat layer. **e** Numerical simulation results of mechanical stresses at the microstructures of the sensor with a single dielectric layer in response to deformation. To accurately reflect the real device structure, where the microstructured pattern is periodically repeated across the sensor, and more precisely analyze the stress concentration, we incorporated periodic boundary conditions in the finite element simulation.

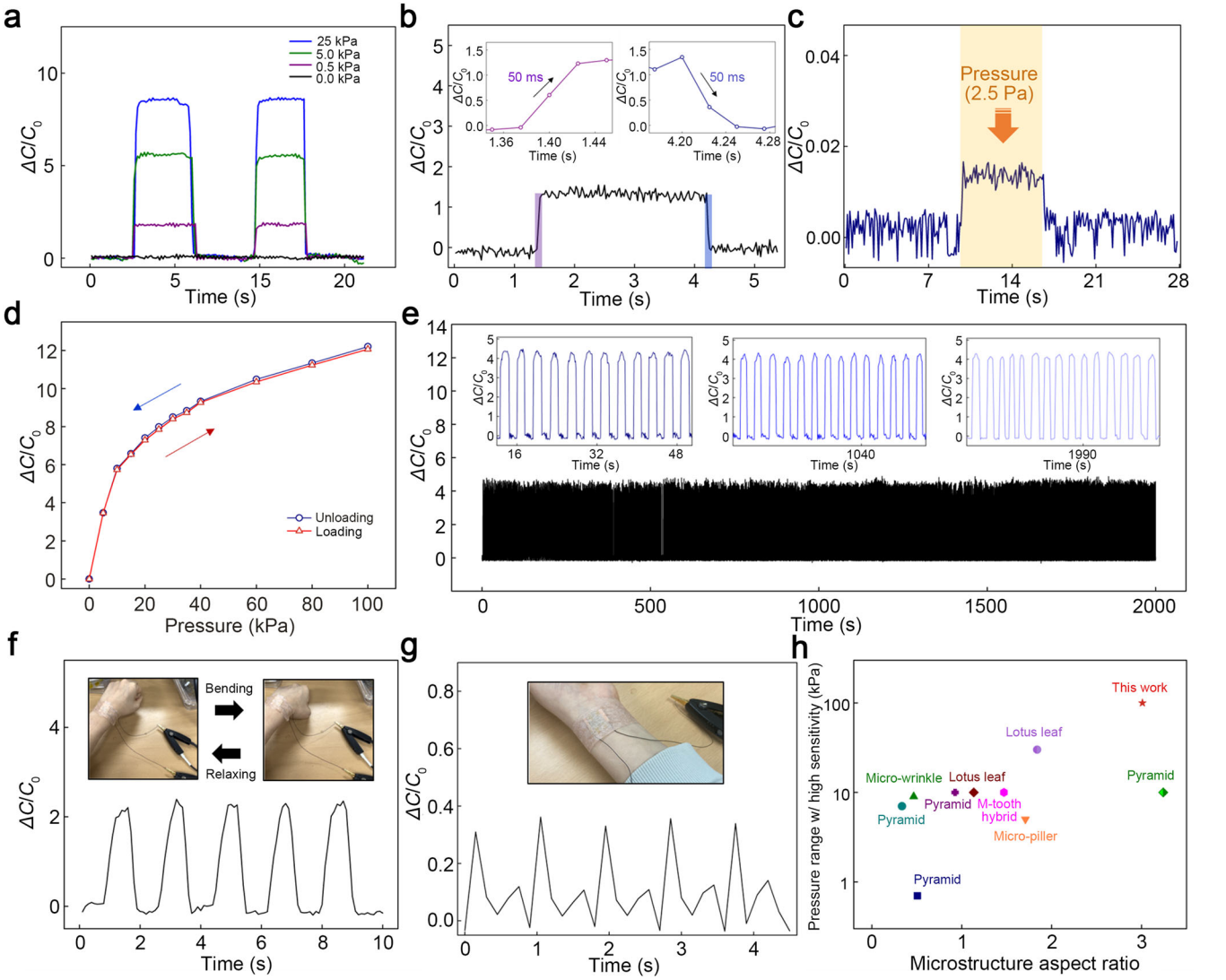

Fig. 2 | Characterization of hourglass-shaped microstructured capacitive pressure sensors. a Normalized capacitive response of the sensor under pressures of 0.0, 0.5, 5.0, and 25 kPa. **b** Response and relaxation times of the pressure sensor at 0.35 kPa. **c** Relative capacitance change under a slight pressure of 2.5 Pa. **d** Normalized capacitive response during the loading/unloading cycle from 0 to 100 kPa. **e** Long-term stability of the sensor over 1100 loading/unloading cycles at 4.50 kPa. Capacitance variations corresponding to (**f**) wrist and (**g**) radial artery pulses. **h** Comparison of aspect ratios for microstructures and pressure ranges with high sensitivity (>0.5 kPa^{-1}) in the proposed sensors versus previously reported devices incorporating microstructured films.

designed to focus stress in the thinner midsections, similar to the starfish surface (Fig. 1c). Figure 1d shows the normalized capacitive responses of pressure sensors comprising single and double layers of the starfish-inspired microstructured films, as well as a reference sensor with a flat dielectric film. To characterize the capacitive responses of the pressure sensors, we used a measurement system comprising an LCR meter, a highly accurate mechanical testing apparatus, and a processing computer (Supplementary Fig. 2). Compared to the reference device, the sensors with microstructured films exhibited significantly higher sensitivity across the pressure range of 0 to 100 kPa. When the sensitivity (S) was calculated as $S = \delta(\Delta C/C_0)/\Delta P$, where $\Delta C = (C - C_0)$ and ΔP represent the capacitance change under pressure stimulus and the applied pressure intensity, respectively, the most sensitive device, a sensor with the single microstructured layer, exhibited three linear regions with distinct S values. The average S values for pressures below 0.5 kPa (low-pressure regime), within the range of 0.5–10 kPa (medium-pressure regime), and above 10 kPa (high-pressure regime) are approximately 2.81, 0.43, and 0.06 kPa^{-1}, respectively (Supplementary Fig. 3a). In the device, mechanical stresses concentrated on the microstructures become more evenly distributed across the entire area as pressure transitions from the low to high regime. This phenomenon is associated with the bending deformation of the structures, leading to saturation of the resulting capacitance change in response to external stimuli (Fig. 1e). These behaviors are consistent with other sensors composed of microstructured dielectric films[22,23]. Engineered with high-aspect-ratio, hourglass-shaped micropillars that focus stress and accommodate mechanical deformations, the sensor structure achieved both high sensitivity and structural stability, enabling a notably wider detection range and exceptional responsiveness under varying pressures[24], compared to devices with conventional micropillar structures of the same aspect ratio (Fig. 1e and Supplementary Fig. 4). Additionally, the pressure sensor with the double microstructured layers exhibited lower sensitivity compared to the single-layered sensor, due to the increased microstructure density, which limits the deformation of the structures[24] (Supplementary Figs. 3b and 5).

We analyzed the sensing performance of the developed pressure sensor, which incorporates a single microstructured layer, to assess its feasibility for integration into a tactile sensory nerve system. To evaluate the dynamic response of the sensor, we measured the relative capacitance changes during repeated loading and unloading cycles under pressures of 0, 0.5, 5.0, and 25 kPa (Fig. 2a). The device exhibited reversible and reproducible responses across all pressure conditions, confirming its reliability in detecting

mechanical stimuli. Moreover, the starfish-inspired sensor detected an external stimulus (0.35 kPa) with a rapid response and relaxation time of less than 50 ms, demonstrating reliable dynamic responses (Fig. 2b)[18,22]. The detection limit is a crucial parameter that dictates the potential applications of a pressure sensor. The capacitive sensor precisely detected minute pressures as low as 2.5 Pa, demonstrating a low detection limit (Fig. 2c) and making it highly promising for applications requiring exceptional sensitivity to delicate signals. We also tested the stability of the sensors, as presented in Fig. 2d, e. During loading and unloading tests over a wide pressure range (0 to 100 kPa), the sensor exhibited minimal hysteresis while maintaining high stability. Over 1100 loading and unloading cycles under 4.50 kPa, the sensor demonstrated stable performance without noticeable degradation, showcasing long-term durability comparable to that of other sensors[23,25]. In addition, the device exhibited high durability against temperature variations, attributed to its sensing mechanism based on capacitive changes[26] (Supplementary Fig. 6).

With its high sensitivity, reliability, and stable sensing performance in detecting pressure stimuli, the sensor is well-suited for practical applications, including the detection of body movements and arterial pulse signals. The capacitive pressure sensor, when attached to the user, accurately monitored repeated wrist movements and arterial pulse signals (Fig. 2f, g). Moreover, the pressure sensing properties exhibited significant reproducibility, highlighting the strong potential for integration into advanced sensing systems (Supplementary Fig. 7). The eight different pressure sensors demonstrated high uniformity with minimal cell-to-cell variation, quantified as the ratio of the standard deviation to the mean capacitance (0.01, 0.02, and 0.02 at 0.35, 3.5, and 35 kPa, respectively). Furthermore, the sensors operated stably regardless of cell area, confirming their suitability for practical applications in large-scale sensor arrays (Supplementary Fig. 8). Although the sensitivity of the developed sensor was lower in the low-pressure range than that of micro-pyramidal structured sensors with the same aspect ratio, due to their smaller shape factor, our sensor effectively responded to subtle pressures below 1 kPa as well as deep pressures up to 100 kPa, surpassing the limited sensing range (0–10 kPa) of the pyramidal microstructured sensor[25,27] (Supplementary Table 1). Moreover, the developed starfish-inspired sensors, derived from natural biological templates, offer a scalable and cost-effective fabrication approach, eliminating the need for intricate processing steps compared to sensors with micro-pyramid structures fabricated via complex techniques for the high aspect ratio. In terms of the microstructure aspect ratio and detectable sensing range, both key factors in mimicking biological tactile systems, the starfish-inspired pressure sensor exhibits remarkably superior performance. With a sensitivity exceeding 0.06 kPa^{-1}, it outperforms other pressure sensors incorporating microstructured PDMS layers[19,22,23,25,28–32], highlighting its high sensitivity across a wide stimulus range (Fig. 2h). These exceptional performance characteristics suggest the sensor's strong potential as an effective tactile sensory receptor.

Flexible memristors with neuronal functions

Memristors exhibiting resistive switching behaviors are promising candidates for artificial sensory neurons due to their controllable memory volatility, making them well-suited for emulating neuronal functions[33,34]. We fabricated flexible memristors based on the electrochemical metallization (ECM) phenomenon, using silver as the active electrode for ion generation and poly(vinyl cinnamate) as the polymer medium to facilitate ion migration paths[34,35] (Fig. 3a). The prepared memristor was initialized through an electroforming process for triggering the conductive filament (CF) formation (Supplementary Fig. 9a). The device exhibited reliable resistive switching characteristics under different compliance current (CC) conditions of 10^{-5}, 4×10^{-5}, and 9×10^{-5} A (Fig. 3b). As the CC increased from 10^{-5} A to 4×10^{-5} A, the holding voltage of the device, which initially exhibited volatile characteristics, decreased from 0.15 V to 0.05 V. At a CC of 9×10^{-5} A, the device operated as non-volatile memory (Supplementary Fig. 9b), with an on/off current ratio of approximately 10^4. During retention testing, the memory stability of the device in the low-resistance state (LRS) improved with increasing the CC (Fig. 3c). These results indicate a transition from volatile to non-volatile memory behaviors in the memristor, driven by the CC. In the ECM memristors, the CF growth is constrained by the CC, which governs the filament stability and the resulting memory volatility[36,37]. Throughout the switching process, the prepared memristor exhibited space charge-limited conduction, characterized by Ohmic behavior, Child's law, and an abrupt increase in conductance, indicating CF growth based on the ECM phenomenon[38] (Supplementary Fig. 10).

To precisely confirm the operating principle of the memristor, we analyzed the effects of cell size and temperature variations on its resistive switching characteristics[39,40]. Despite the increase in cell area, the device exhibited reproducible resistive switching behavior, with only a slight increase in leakage current in the high-resistance state (HRS) (Supplementary Fig. 11). This suggests that the resistive switching characteristics of the device are primarily governed by filamentary conduction through the CFs. Additionally, the device in the LRS exhibited a negative temperature coefficient of conductivity, indicating that the conductance changes are attributed to the metal-atom-based CFs (see Supplementary Fig. 12). Figure 3d illustrates the CF growth and the resistive switching behavior of the device, in response to electrical stimuli. When the electrical stimulus is insufficient to form the stable CFs, the memristor switches from the HRS to the medium resistance state (MRS), which is higher than the LRS. In the MRS, the device conductance gradually returns to the HRS due to the self-dissolution of the unstable CFs. In contrast, once the electrical stimulus is large enough for the stable CF formation, the device transitions to the LRS, and an additional reset process, involving a negative voltage signal, is required to rupture the CFs and revert to the HRS. Such tunable memory volatility in the memristors can serve as a useful tool for replicating various biological sensory neurons[41].

To develop practical artificial sensory neurons, it is essential to emulate neuronal functions under pulsed operations. We demonstrated STP and LTP in the flexible memristor using the 20-μs voltage pulses with amplitudes of 1.5 V and 2.5 V, respectively (Supplementary Fig. 13). The device exhibited a transient increase in conductance, analogous to STP, in response to a lower voltage pulse of 1.5 V, while a larger pulse of 2.5 V induced a sustained increase in conductance, mimicking LTP. Under repeated voltage pulses with insufficient amplitude to form the stable CFs, the device exhibited a temporary peak current that increased with the number of pulses, demonstrating the STP function of paired-pulse facilitation (Supplementary Fig. 14). Moreover, the device exhibited multilevel conductance states, similar to LTP characteristics, under optimized successive 10-μs pulses ranging from 2.4 to 3.8 V for the set process and −2.4 to −3.8 V for the reset process (Fig. 3e). These biomimetic functions allow the developed memristors to serve as artificial sensory neurons, facilitating near-sensor computing applications.

As an artificial sensory neuron suitable for wearable electronics, electrical and mechanical stability are essential features of flexible memristors[41–43]. We first measured the electrical durability of the device through cycle tests involving voltage sweeps for the set and reset processes (Fig. 3f). Over 300 cycles, the device exhibited stable and reliable characteristics, similar to other artificial synaptic devices[44,45]. We further analyzed the reproducibility of the device's resistive switching by estimating the temporal variations in set and reset voltages during the cycle tests (Fig. 3g). The temporal variations, calculated as the ratio of the standard deviation to the average value, were approximately 0.13 and −0.17 for the set and reset voltages, respectively, indicating the reproducible switching performances of the device, comparable to that of the conventional ECM memristors[38,46,47]. Moreover, the twenty different cells in the 4×5 memristor array exhibited minimal variation in switching voltages during the set and reset processes, with a spatial variation parameter, defined as the ratio of the standard deviation to the mean, of 0.20 for both processes, demonstrating the consistency of memristor fabrication[34] (Supplementary Fig. 15). The distributions in reproducibility and device-to-device uniformity of the memristors mainly arise from the stochastic growth of the CFs and can be significantly improved by inducing localized ion injection[35,48]. To assess the mechanical endurance of the flexible memristor, we investigated its resistive switching

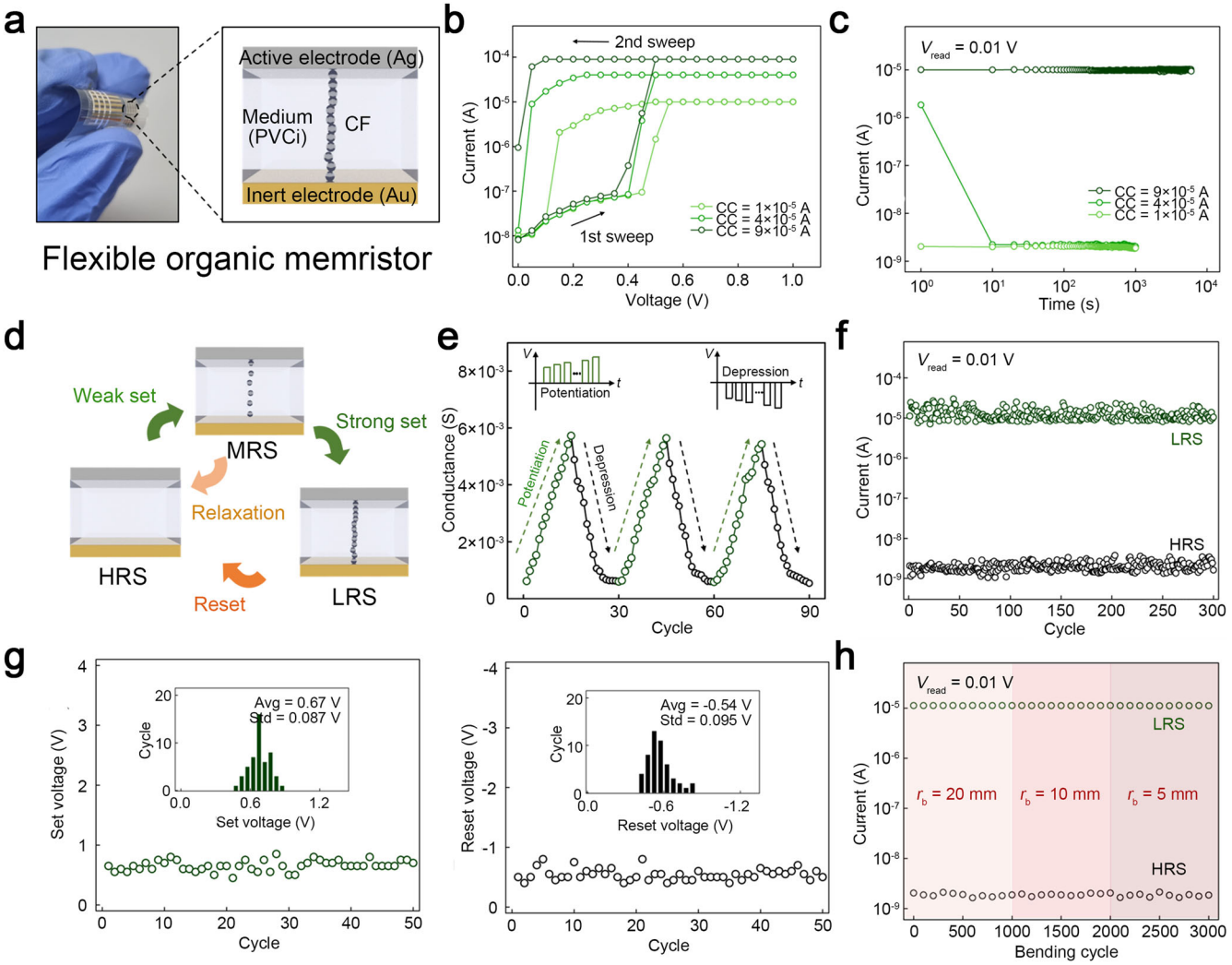

Fig. 3 | Development of flexible memristors for artificial sensory neurons. **a** Photograph of the flexible memristor arrays, with an inset displaying the device configuration. **b** Current−voltage characteristics of the device under different compliance current (CC) conditions: 1×10^{-5}, 4×10^{-5}, and 9×10^{-5} A. **c** Memory retention performance of the device after programming at each CC. **d** Schematic illustrating the device's operating principles, replicating neuronal functions such as short-term and long-term plasticity (STP and LTP). **e** Multilevel conductance states of the device in pulse operation mode. **f** Cycle tests under voltage sweeps, evaluating the device's electrical endurance. **g** Dispersion in set and reset voltages over 50 successive cycles. **h** Resistive switching characteristics of the device under positive bending states for varying bending radii (r_b) values: 20, 10, and 5 mm.

behavior under bending deformation stress. The device exhibited stable resistive switching behavior and reliable operations, regardless of the repeated bending stresses at various bending radius (r_b) values (Fig. 3h and Supplementary Fig. 16). Furthermore, the device's conductance states at both the HRS and LRS were maintained for over 3000 s under bending deformations with a r_b of 5 mm (Supplementary Fig. 17). This remarkable mechanical durability of the flexible memristor suggests its strong potential for use in practical wearable systems.

Energy-efficient artificial sensory nerves for nociceptive applications

Tactile nociceptors are sensory nerves responsible for detecting and perceiving high-intensity mechanical stimuli that cause pain[49,50]. In the nociceptors, an external stimulus that exceeds a specific threshold induces an action potential signal for transmission to a central nervous system. For the practical application of artificial nociceptors in wearable electronics, achieving energy-efficient operation of the systems is critical. The capacitive pressure sensor integrated with a flexible memristor, functions as an artificial sensory nerve, mimicking a nociceptor and offering high energy efficiency (Fig. 4a). We developed a tactile sensory nervous system composed of a capacitive pressure sensor and a flexible memristor, serving as the sensory receptor and neuron, respectively (Fig. 4b). Upon application of triangle-wave pulses to the artificial sensory nerves, the capacitive pressure sensor generated a displacement current exclusively during its charging phase, producing a temporary electric potential across the memristor. The high sensitivity of the hourglass-shaped microstructured pressure sensor allowed modulation of the amplitude and duration of the electric potential at the memristor in response to the applied pressure stimulus. Furthermore, incorporating a 33 kΩ load resistor enhanced the sensitivity of potential changes at the memristor to variations in sensor capacitance (Supplementary Fig. 18) by reducing the memristor's equivalent resistance.

To demonstrate the nociceptor functions within the system, we applied 6 V reading pulse signals with rising and falling times of 150 ns and 3 µs, respectively. We set the pulse period to 1 second to match the duration of external pressure stimuli, enabling highly energy-efficient operation. Given that the minimum sampling time, defined by the reading pulse, is approximately 3 µs, the operating frequency of the system can be adjusted from approximately 333 kHz to lower sampling rates. As pain-sensory nerves, the nociceptor system must adhere to four key principles: threshold, relaxation, no adaptation, and sensitization[15,49]. The developed sensory

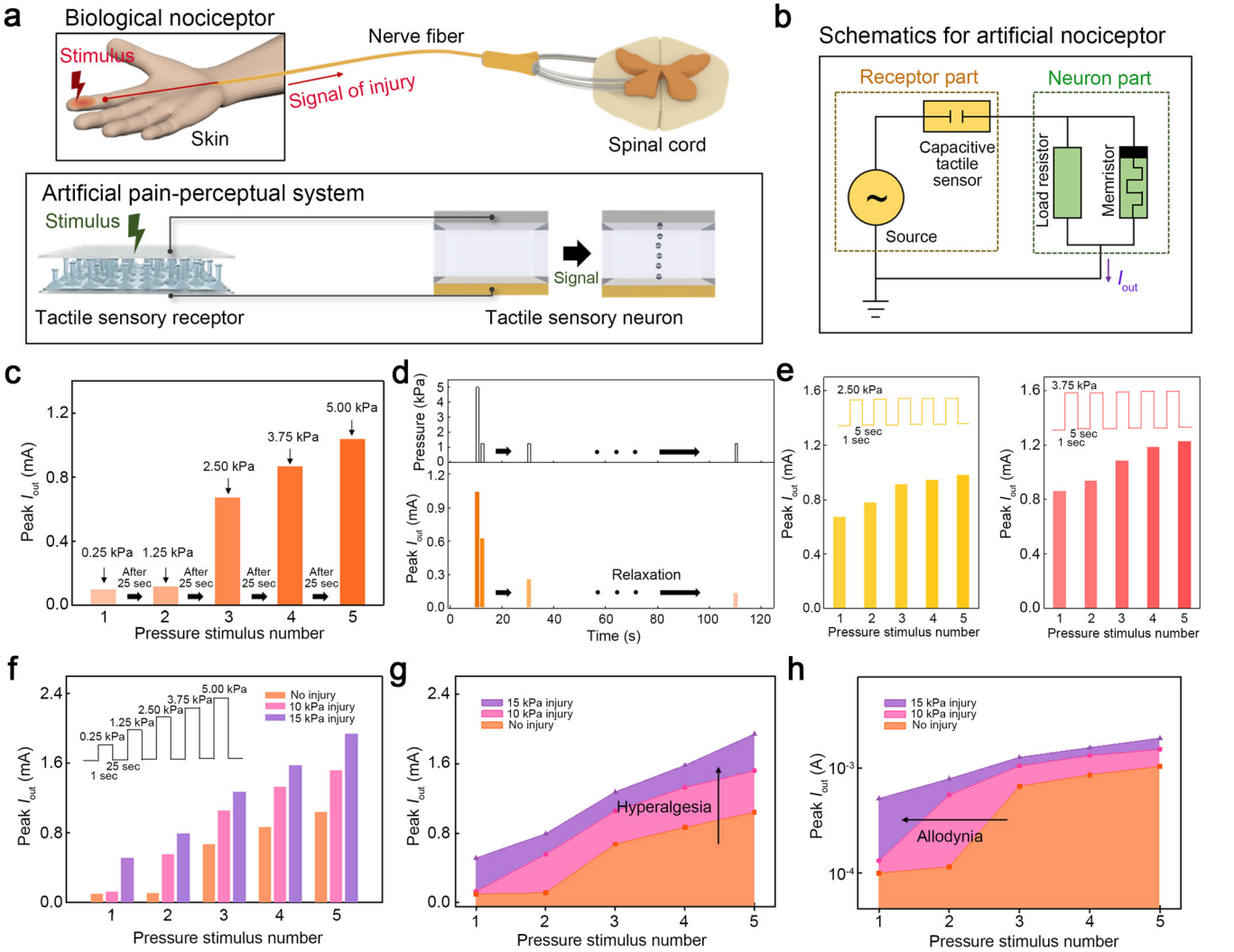

Fig. 4 | Artificial sensory nerve, functioning as a nociceptor with high energy efficiency. a Concept of the artificial nociceptor comprising hourglass-shaped microstructured capacitive pressure sensor and a flexible memristor. In this system, the pressure sensor and flexible memristor play as a tactile sensory receptor and neuron, respectively. **b** A circuit diagram for the nociceptor. A load resistor of 33 kΩ offers the sensitive changes of the electric potential at the memristor, in response to variations in the sensor's capacitance. **c** Threshold characteristics of the nociceptor where input pressure pulses 1 s wide with different pulse amplitudes (0.25, 1.25, 2.50, 3.75, and 5.00 kPa). The interval between the pressure stimuli was 25 s. **d** Relaxation characteristics of the system. After application of 5.00 kPa pressure stimulus, a 1.25 kPa pressure pulse with different interval times was applied. **e** No adaptation properties of the system. A sequence of pressure pulses with 2.50 and 3.75 kPa was utilized. **f** Responses of the uninjured (0 kPa) and injured (10 and 15 kPa) systems to the input pressure stimuli composed of different amplitudes (0.25, 1.25, 2.50, 3.75, and 5.00 kPa). **g** Hyperalgesia and (**h**) Allodynia characteristics represented in the nociceptor system.

nervous system exhibited threshold-triggering behavior in response to pressure stimuli, gradually varying from 0.25 to 5.00 kPa, with a duration of 1 s and intervals of 25 s (Fig. 4c and Supplementary Fig. 19). When the pressure exceeded 2.50 kPa, the output peak current of the artificial sensory nerve rose abruptly, from approximately 114 μA to over 673 μA, due to resistive switching in the memristor, mimicking the biological threshold linking stimulus intensity to perceived nociceptive response.

In natural nociceptors, the triggered signal dissipates once the noxious stimulus is removed[15,49,50]. We tested this nociceptive relaxation in our system by measuring changes in peak current following the application of a threshold-level noxious stimulus (5.00 kPa) (Fig. 4d and Supplementary Fig. 20). Following a noxious stimulus, repeated subthreshold stimuli (1.25 kPa) gradually led the peak current in the system to return to its initial state. This effect, attributed to the STP functions of the memristor, became more pronounced as the interval between threshold and subthreshold stimuli increased, indicating a stable relaxation function.

Another important feature of nociceptors is their lack of adaptation to continuous harmful stimuli[15,49,50]. Under successive pressure stimuli at intensities of 2.50 and 3.75 kPa, the system maintained output peak current levels regardless of stimulus number, with higher current responses observed at higher pressure levels (Fig. 4e and Supplementary Fig. 21). This behavior aligns with the non-adaptive response of its biological counterpart.

Sensitization is critical for an effective response to nerve injury[15,49,50]. This function encompasses a reduction in the stimulus threshold, leading to allodynia, and an enhancement in nociceptor response, resulting in hyperalgesia, following the injury. To verify the sensitization feature in the developed nociceptor, we induced different injury conditions by applying pressures of 10.00 and 15.00 kPa, respectively, and subsequently applied successive pressures with increasing amplitudes (from 0.25 to 5.00 kPa, 1 s duration) to the system (Fig. 4f–h, and Supplementary Fig. 22). Compared to the initial, uninjured system, the injured systems showed increased responses to applied pressures and a decreased stimulus threshold for pain. This sensitization behavior became more evident with increasing injury severity. In the replotted peak current values from Fig. 4f, corresponding to successive pressure increments, the response peak current in the injured states was higher than that in the initial, uninjured state. Moreover, the peak

current values increased with the magnitude of the injury pressure (Fig. 4g), clearly demonstrating hyperalgesia. Additionally, the threshold pressure required to trigger a response current decreased from 2.50 kPa to 1.25 kPa and 0.25 kPa after exposure to injury stimuli of 10.00 kPa and 15.00 kPa, respectively. This behavior is consistent with allodynia observed in natural nociceptors (Fig. 4h). These sensitization characteristics of our system are attributed to the STP properties of the memristor in the neuronal component[50]. As the pressure at the sensory interface increases, the electrical signal at the memristor is amplified (Supplementary Fig. 18), promoting the growth of CFs for resistive switching and extending its retention time. Consequently, a sufficiently high pressure that induces CF growth, sustaining for over 25 s, enhances the response to applied pressures and lowers the stimulus threshold for pain perception in the nociceptor system. Given that a pressure stimulus of 5.00 kPa is insufficient to generate a prolonged response lasting 25 s (Fig. 4d), we conclude that higher pressure stimuli, such as 10.00 and 15.00 kPa, are appropriate injury conditions.

In addition to the nociceptive principles of threshold, relaxation, non-adaptation, and sensitization, the developed system also implemented a treatable injury state[14] (Supplementary Figs. 23 and 24). When a mechanical stimulus of 30.00 kPa was applied to the system for 1 s, the conductance state of the memristor transitioned to the low-resistance state (LRS) with non-volatile properties, leading to an increase in peak current associated with the induced injury. This injured state was sustained permanently, indicating the need for a recovery treatment to restore the nociceptor to its pristine, uninjured state. As the restoration treatment to reset the memristor, we applied a pressure of 1.25 kPa along with 8 V triangle-wave pulses, featuring rising and falling times of 3 μs and 150 ns, respectively, and a pulse period of 1 s. The discharging effect of the capacitive sensor provided a negative electric potential to the memristor, switching the sensory neuron resistance from the LRS to the HRS and thereby enabling the recovery of the nociceptor to its uninjured state.

Unlike other artificial nociceptors composed of resistive pressure sensors, the developed sensory nervous system, based on a capacitive receptor, uses the transient electric field generated during the sensor's charging process to govern the resistive switching behaviors of the neuronal memristor components. Consequently, the system operates with significantly higher energy efficiency than those in previous studies[14,15,51–53] (Supplementary Fig. 25 and Table 2), demonstrating promising potential for practical near-sensor computing.

Tactile near-sensor computing with bio-realistic energy efficiency

A near-sensor computing system serves as a valuable tool for real-time acquisition and processing of environmental data[4,5], supporting the development of advanced portable and wearable electronics. To evaluate the potential of the developed artificial tactile nervous system, which comprises starfish-inspired pressure sensors and flexible memristors, for near-sensor computing, we designed the system to monitor fingerprint pressures and process signals for noise reduction (Fig. 5a). We used SPICE simulations to estimate system performance and configured the memristor-sensor array as a 3 × 3 mean filter for a single fingerprint pixel (Fig. 5b). Each memristor was trained to the LRS state with 1.58 kΩ for mean computation, and a 100 Ω load resistor was connected to the filter to monitor the summed current. For real-time detection and computation of fingerprint signals across 60 × 60 pixels, we utilized a triangular 0.01 V pulse with a 10 ns rising time and a 2 μs falling time to monitor pressure stimuli of 4 kPa (Fig. 5c). When the voltage across the load resistor of the filter exceeded 0.0016 V, the pixel was classified as being in a pressed state. The constructed system reliably processed noisy fingerprint images for denoising, generated with additive white Gaussian noise[54] at a σ value of 110 (Fig. 5d). Across 20 repeated tests with randomly generated noisy images, the denoised signals achieved high matching accuracy, about 93%, with the original fingerprint signals (Supplementary Fig. 26 and Table 2). When calculating the energy consumption for a single pixel by extracting voltage pulse and current values from the nine filter lines through the SPICE simulations (Supplementary Fig. 27), the system, on average, consumed approximately 8 pJ for processing 60 × 60 pixel signals and 2.2 fJ per pixel, closely approaching biological energy levels[55,56] (Fig. 5e).

Furthermore, we demonstrated the computing capabilities of the artificial sensory nerves for edge detection (Fig. 5f). We used the same structure as the system for denoising the signals. We configured the memristor resistance for weights of "1" and "−1" at the LRS with 175 Ω, and for "0" at 1.63 kΩ. We then applied a triangular 0.1 V pulse with a 10 ns rising time and a 2 μs falling time to monitor pressure signals of 4 kPa, adjusting the voltage polarity to reflect a negative weight in the memristor. To convert the analog edge-detected signals to binary data, we compared the average intensity of the load voltages for horizontally and vertically edge-detected pixels against a threshold of 0.0083 V, representing the minimum voltage required to confirm an edge pixel. The system achieved effective operation for edge detection with low energy consumption (Fig. 5g). These results highlight the high capability of the developed tactile sensory nerves, making them suitable for compact, practical applications that require high energy efficiency.

Discussions

We proposed a robust approach to achieve artificial tactile nerves with bio-realistic energy efficiency, paving the way for near-sensor computing systems adaptable to real-world portable and wearable electronic applications. A capacitive pressure sensor with high sensitivity across a wide stimulus range was developed as a tactile sensory receptor by introducing hourglass-shaped, high-aspect-ratio microstructures into the dielectric film. Additionally, we implemented controllable memory volatility in a flexible memristor, enabling the STP and LTP functions essential for emulating biological sensory neurons. The artificial tactile sensory nervous system, integrating hourglass-shaped microstructured capacitive sensors and flexible memristors, exhibited energy efficiency close to biological levels. This remarkable efficiency arises from the transient transduction of mechanical stimuli into electric potential through the capacitive sensor charging process. Furthermore, the developed sensory nerves effectively functioned as both artificial nociceptors operating over a large stimulus range (0–30 kPa) and as tactile near-sensor computing systems for a smaller pressure range (0–4 kPa). We anticipate that our strategy will offer significant potential for next-generation neuromorphic systems, positioning them as ideal candidates for portable and wearable electronics. These efforts constitute a substantial contribution to the realization of bio-realistic artificial intelligence systems in the coming years.

Methods

Hourglass-shaped microstructured capacitive pressure sensors fabrication

To prepare a master mold for a dielectric film featuring hourglass-shaped microstructures, we affixed a rectangular section of the starfish surface onto a glass substrate and poured a PDMS (Sylgard 184, Dow Corning Corp.) mixture with a 10:1 base-to-curing agent ratio over the starfish surface. After curing at 70 °C for 2 h, the PDMS film with inverse starfish structures was peeled off to serve as a master mold template. We then coated the mold template with a fluorinated polymer (Novec™ EGC-1700, 3 M) to reduce its adhesion. We carried out the molding process for a microstructured dielectric film following the same steps used to create the master mold template. Using the prepared master mold template, we fabricated a PDMS film featuring microstructures that replicate the starfish surface.

To fabricate the pressure sensors, indium-tin-oxide (ITO)-patterned polyethylene naphthalate (PEN) substrates were first cleaned sequentially using ultrasonication in acetone, isopropyl alcohol, and deionized water for 30 min each. The two PEN substrates were then assembled with the ITO layers oriented perpendicularly to each other, with the microstructured PDMS film inserted between them. Prior to attaching the microstructured film to the substrates, we performed a 5-minute ultraviolet ozone treatment to enhance its adhesion. Finally, we bonded the edges of the sensor using Kapton tape to enhance structural stability. The active area of the cell size in the sensor was 2 × 2 cm^2.

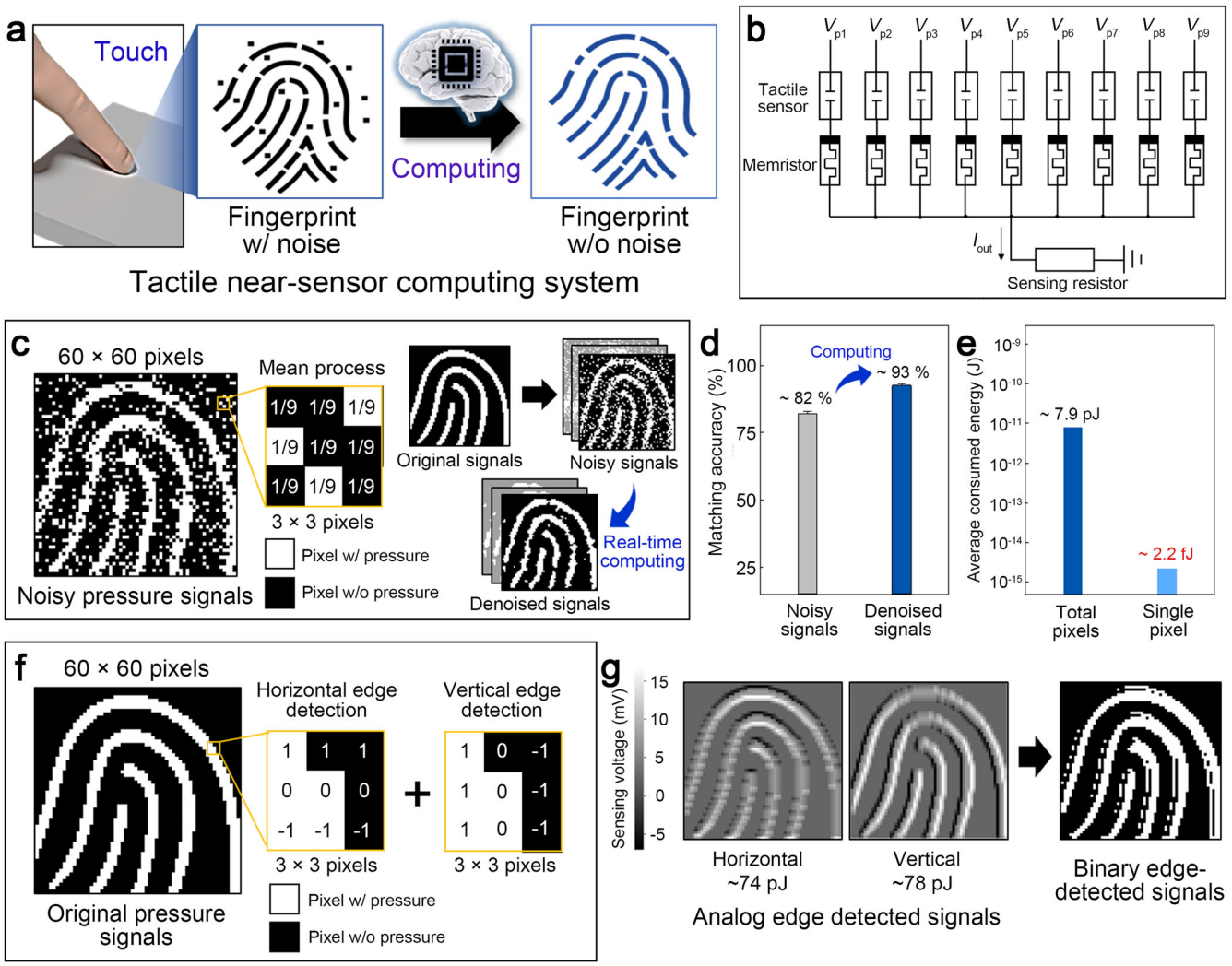

Fig. 5 | Tactile near-sensor computing for real-time sensing and processing of pressure stimuli, integrating hourglass-shaped microstructured capacitive sensors and flexible memristors. a Conceptual illustration of the near-sensor computing system for noise reduction in fingerprint stimuli. **b** System configuration of a 3 × 3 mean filter for processing a single fingerprint pixel. **c** Schematic representation of processing noisy fingerprint stimuli to yield a denoised signal image in the tactile sensory nerves. For each pixel's denoising, currents from the 3 × 3 pressure sensors were averaged using the mean filter. **d** Pixel bit matching accuracy between the original fingerprint image and the noisy or processed signals in the near-sensor computing. **e** Average energy consumption for denoising 60 × 60 fingerprint signals and a single pixel within the system. **f** Schematic of the edge-detection process for fingerprint stimuli, utilizing the same 3 × 3 filter structure as in mean filtering. **g** Fingerprint signal image generated by edge detection based on pressure stimuli detected within the system.

Flexible memristors fabrication

To fabricate a flexible memristor, a PEN substrate with ITO patterns for the bottom electrodes was sequentially cleaned using ultrasonication in acetone, isopropyl alcohol, and deionized water for 30 min. As a polymer switching layer, we spin-coated a 5 wt.% solution of poly(vinyl cinnamate) dissolved in cyclopentanone onto the substrate at a rate of 3000 rpm for 30 s. We then baked the polymer film at 130 °C for 2 h to remove any residual solvent. The thickness of the switching layer was approximately 280 nm. For the top electrode, we thermally deposited a 50-nm thick silver layer at a rate of 1 Å/s under a vacuum of 10^{-6} Torr. The dimensions of the active cell area were 50 μm × 50 μm.

Characterization

The surface profiles of the films were investigated using a geometrical profiler (DektakXT-A, Bruker). A field-emission scanning electron microscope (S-4800, Hitachi) was employed to analyze the geometrical structures of the starfish-inspired dielectric film.

Using a custom-built high-precision testing system with a z-axis stage and a load cell (UMM-k10, DACELL Korea), we applied controlled pressure stimuli to the sensors. This setup enabled precise measurement of the applied force and displacement, while a high-precision LCR meter (E4980A, Agilent) recorded the corresponding capacitance values, allowing for detailed analysis of the capacitive response under varying pressure conditions.

The electrical performances of the flexible memristors and the nervous systems were measured using a semiconductor parameter analyzer (4200-SCS, Keithley) integrated with an ultrafast I–V module (4225-PMU, Keithley). To investigate the electrical characteristics of the memristors, we applied scanning voltage signals to the silver top electrode while grounding the ITO bottom electrode.

Numerical simulations for sensors and near-sensor computing operations

We utilized COMSOL software to analyze the deformation behavior of the pressure sensors. The simulation model was constructed to reflect the actual dimensions of the fabricated sensors. We employed a Mooney-Rivlin model with hyperelastic properties to describe the material characteristics of the dielectric layer. To accurately reflect the real device structure, where the microstructured pattern is periodically repeated across the sensor, and more

precisely analyze the stress concentration, we incorporated periodic boundary conditions in the finite element simulation.

We used a LTspice tool to construct and analyze the near-sensor computing systems. In modeling filters for the denoising process and edge detection, we configured resistors and capacitors to match the target conductance of the memristors and the capacitance states of the sensors, serving as sensory neurons and receptors.

Data availability

The authors declare that data supporting the findings of this study are available within the article and its Supplementary Information files.

Code availability

Code available from the corresponding author upon reasonable request.

Received: 20 January 2025; Accepted: 22 April 2025;
Published online: 01 May 2025

References

1. Jung, U., Beak, C.-J., Kim, K., Na, J.-H. & Lee, S.-H. Scalable photo-responsive physical unclonable functions via particle kinetics. *ACS Nano* **18**, 27642–27653 (2024).
2. Dai, S. et al. Intrinsically stretchable neuromorphic devices for on-body processing of health data with artificial intelligence. *Matter* **5**, 3375–3390 (2022).
3. Lee, H. E. et al. Novel electronics for flexible and neuromorphic computing. *Adv. Funct. Mater.* **28**, 1801690 (2018).
4. Du, Y. et al. Monolithic 3D integration of analog RRAM-based computing-in-memory and sensor for energy-efficient near-sensor computing. *Adv. Mater.* **36**, 2302658 (2024).
5. Zhou, F. & Chai, Y. Near-sensor and in-sensor computing. *Nat. Electron.* **3**, 664–671 (2020).
6. Jang, H. et al. Flexible neuromorphic electronics for wearable near-sensor and in-sensor computing systems. *Adv. Mater.* **37**, 2416073 (2025).
7. Wang, H. et al. A ferroelectric/electrochemical modulated organic synapse for ultraflexible, artificial visual-perception system. *Adv. Mater.* **30**, 1803961 (2018).
8. Zang, Y., Shen, H., Huang, D., Di, C.-A. & Zhu, D. A dual-organic-transistor-based tactile-perception system with signal-processing functionality. *Adv. Mater.* **29**, 1606088 (2017).
9. Zhang, Y. et al. Near-sensor analog computing system based on low-power and self-assembly nanoscaffolded $BaTiO_3$:Nd_2O_3 memristor. *Nano Today* **55**, 102144 (2024).
10. Huang, J. et al. A bioinspired MXene-based flexible sensory neuron for tactile near-sensor computing. *Nano Energy* **126**, 109684 (2024).
11. Chen, S., Lou, Z., Chen, D. & Shen, G. An artificial flexible visual memory system based on an UV-motivated memristor. *Adv. Mater.* **30**, 1705400 (2018).
12. Lee, Y., Oh, J. Y. & Lee, T.-W. Neuromorphic skin based on emerging artificial synapses. *Adv. Mater. Technol.* **7**, 2200193 (2022).
13. Yu, J. et al. Bioinspired mechano-photonic artificial synapse based on graphene/MoS_2 heterostructure. *Sci. Adv.* **7**, eabd9117 (2021).
14. Du, S. et al. An artificial universal tactile nociceptor based on 2D polymer film memristor arrays with tunable resistance switching behaviors. *ACS Appl. Mater. Interfaces* **16**, 33907–33916 (2024).
15. Tsao, S.-C. et al. Heterogeneous integration of memristive and piezoresistive MDMO-PPV-based copolymers in nociceptive transmission with fast and slow pain for an artificial pain-perceptual system. *Small* **20**, 2311040 (2024).
16. Wang, M. et al. Tactile near-sensor analogue computing for ultrafast responsive artificial skin. *Adv. Mater.* **34**, 2201962 (2022).
17. Gerratt, A. P., Michaud, H. O. & Lacour, S. P. Elastomeric electronic skin for prosthetic tactile sensation. *Adv. Funct. Mater.* **25**, 2287–2295 (2015).
18. Wu, L. et al. Beetle-inspired gradient slant structures for capacitive pressure sensor with a broad linear response range. *Adv. Funct. Mater.* **34**, 2312370 (2024).
19. Wan, Y. et al. A highly sensitive flexible capacitive tactile sensor with sparse and high-aspect-ratio microstructures. *Adv. Electron. Mater.* **4**, 1700586 (2018).
20. Jin, Y., Shen, H., Sun, L., Zhou, X. & Chen, L. Multilevel nanostructured pressure sensor for object recognition with Deep-Learning assistance: A strategy for high sensitivity and wide detection range. *Chem. Eng. J.* **484**, 149298 (2024).
21. Asghar, W. et al. Piezocapacitive flexible E-Skin pressure sensors having magnetically grown microstructures. *Adv. Mater. Technol.* **5**, 1900934 (2020).
22. Farman, M. et al. All-polydimethylsiloxane-based highly flexible and stable capacitive pressure sensors with engineered interfaces for conformable electronic skin. *ACS Appl. Mater. Interfaces* **15**, 34195–34205 (2023).
23. Palaniappan, V. et al. Flexible M-tooth hybrid micro-structure-based capacitive pressure sensor with high sensitivity and wide sensing range. *IEEE Sens. J.* **21**, 26261–26268 (2021).
24. Tee, B. C.-K. et al. Tunable flexible pressure sensors using microstructured elastomer geometries for intuitive electronics. *Adv. Funct. Mater.* **24**, 5427–5434 (2014).
25. Palaniappan, V. et al. Laser-assisted fabrication of a highly sensitive and flexible micro pyramid-structured pressure sensor for E-Skin applications. *IEEE Sens. J.* **20**, 7605–7613 (2020).
26. Zhou, M.-X., Huang, Q.-A., Qin, M. & Zhou, W. A novel capacitive pressure sensor based on sandwich structures. *J. Microelectromech. Syst.* **14**, 1272–1282 (2005).
27. Tang, R. et al. Flexible pressure sensors with microstructures. *Nano Sel.* **2**, 1874–1901 (2021).
28. Zhao, L., Yu, S., Li, J., Song, Z. & Wang, X. Highly reliable sensitive capacitive tactile sensor with spontaneous micron-pyramid structures for electronic skins. *Macromol. Mater. Eng.* **307**, 2200192 (2022).
29. Zhao, L. et al. Biomimetic-inspired highly sensitive flexible capacitive pressure sensor with high-aspect-ratio microstructures. *Curr. Appl. Phys.* **31**, 29–37 (2021).
30. Luo, Y. et al. Flexible capacitive pressure sensor enhanced by tilted micropillar arrays. *ACS Appl. Mater. Interfaces* **11**, 17796–17803 (2019).
31. Ma, L. et al. A highly sensitive and flexible capacitive pressure sensor based on a micro-arrayed polydimethylsiloxane dielectric layer. *J. Mater. Chem. C.* **6**, 13232–13240 (2018).
32. Mannsfeld, S. C. B. et al. Highly sensitive flexible pressure sensors with microstructured rubber dielectric layers. *Nat. Mater.* **9**, 859–864 (2010).
33. Jung, U. et al. Formation of cluster-structured metallic filaments in organic memristors for wearable neuromorphic systems with bio-mimetic synaptic weight distributions. *Adv. Sci.* **11**, 2307494 (2024).
34. Kim, H. et al. Organic memristor-based flexible neural networks with bio-realistic synaptic plasticity for complex combinatorial optimization. *Adv. Sci.* **10**, 2300659 (2023).
35. Park, H.-L., Kim, M.-H., Kim, M.-H. & Lee, S.-H. Reliable organic memristors for neuromorphic computing by predefining a localized ion-migration path in crosslinkable polymer. *Nanoscale* **12**, 22502–22510 (2020).
36. Kim, S. E. et al. Systematic engineering of metal ion injection in memristors for complex neuromorphic computing with high energy efficiency. *Adv. Intell. Syst.* **4**, 2200110 (2022).
37. Lee, S.-H. et al. Organic flexible memristor with reduced operating voltage and high stability by interfacial control of conductive filament growth. *Phys. Status Solidi RRL* **13**, 1900044 (2019).
38. Kim, M.-H. et al. Fluoropolymer-based organic memristor with multifunctionality for flexible neural network system. *npj Flex. Electron.* **5**, 34 (2021).

39. Oh, S. et al. Biodegradable and flexible polymer-based memristor possessing optimized synaptic plasticity for eco-friendly wearable neural networks with high energy efficiency. *Adv. Intell. Syst.* **5**, 2200272 (2023).
40. Kim, H. et al. Definition of a localized conducting path via suppressed charge injection in oxide memristors for stable practical hardware neural networks. *ACS Appl. Mater. Interfaces* **15**, 51444–51452 (2023).
41. Park, H.-L. et al. Flexible neuromorphic electronics for computing, soft robotics, and neuroprosthetics. *Adv. Mater.* **32**, 1903558 (2020).
42. Beak, C.-J., Lee, J., Kim, J., Park, J. & Lee, S.-H. Filamentary-based organic memristors for wearable neuromorphic computing systems. *Neuromorph. Comput. Eng.* **4**, 022001 (2024).
43. Lee, H.-S., Ro, J.-S., Ko, G.-M. & Park, H.-L. Flexible and stretchable synaptic devices for wearable neuromorphic electronics. *Flex. Print. Electron.* **8**, 043001 (2023).
44. Park, M. W. et al. Organizing reliable polymer electrode lines in flexible neural networks via coffee ring-free micromolding in capillaries. *ACS Appl. Mater. Interfaces* **14**, 46819–46826 (2022).
45. Zhao, X. et al. Confining cation injection to enhance CBRAM performance by nanopore graphene layer. *Small* **13**, 1603948 (2017).
46. Chandane, P. T., Dongale, T. D., Patil, P. B. & Tiwari, A. P. Organic resistive switching device based on cellulose-gelatine microcomposite fibers. *J. Mater. Sci.: Mater. Electron.* **30**, 21288–21296 (2019).
47. Ding, W. et al. Graphite microislands prepared for reliability improvement of amorphous carbon based resistive switching memory. *Phys. Status Solidi RRL* **12**, 1800285 (2018).
48. Lee, S.-H., Park, H.-L., Kim, M.-H., Kang, S. & Lee, S.-D. Interfacial triggering of conductive filament growth in organic flexible memristor for high reliability and uniformity. *ACS Appl. Mater. Interfaces* **11**, 30108–30115 (2019).
49. Huang, C.-H. et al. Embedded hybrid-dimensional heterointerface for filament modulation in 2D material-based artificial nociceptor. *Adv. Sci.* **11**, 2401946 (2024).
50. Han, X. et al. Highly transparent flexible artificial nociceptor based on forming-free ITO memristor. *Appl. Phys. Lett.* **120**, 094103 (2022).
51. Wang, Y. et al. Flexible Zn-TCPP nanosheet-based memristor for ultralow-power biomimetic sensing system and high-precision gesture recognition. *Adv. Funct. Mater.* **34**, 2316397 (2024).
52. Yan, X. et al. An artificial synapse based on La:$BiFeO_3$ ferroelectric memristor for pain perceptual nociceptor emulation. *Mater. Today Nano* **22**, 100343 (2023).
53. Ge, J., Zhang, S., Liu, Z., Xie, Z. & Pan, S. Flexible artificial nociceptor using a biopolymer-based forming-free memristor. *Nanoscale* **11**, 6591–6601 (2019).
54. Liu, W. & Lin, W. Additive white Gaussian noise level estimation in SVD domain for images. *IEEE Trans. Image Process.* **22**, 872–883 (2013).
55. Lee, Y., Park, H.-L., Kim, Y. & Lee, T.-W. Organic electronic synapses with low energy consumption. *Joule* **5**, 794–810 (2021).
56. Marković, D., Mizrahi, A., Querlioz, D. & Grollier, J. Physics for neuromorphic computing. *Nat. Rev. Phys.* **2**, 499–510 (2020).

Acknowledgements

This work was supported by the National R&D Program through the National Research Foundation of Korea (NRF), funded by the Ministry of Science and ICT (No. RS-2023-00277635). This work was supported by the National Research Foundation of Korea (NRF) grant funded by the Korea government (MSIT) (No. RS-2024-00411764). This work was supported by a grant of the Basic Research Program funded by the Korea Institute of Machinery and Materials (grant number: NK254H), and the Technology Innovation Program (RS-2024-00443121) funded By the Ministry of Trade Industry & Energy (MOTIE, Korea).

Author contributions

J.-Y.C. and S.-H.L. conceived the idea. J.-Y.C., S.E.K., J.L., and S.-H.L. performed all the experimental measurements. J.-Y.C., C.-J.B., W.S., B.-Y.L., and S.-H.L. carried out all the numerical simulations. J.-Y.C., S.E.K., and W.S. fabricated all the samples. B.-Y.L. and S.-H.L. supervised the project. All the authors discussed the results and edited the manuscript.

Competing interests

The authors declare no competing interests.

Additional information

Supplementary information The online version contains supplementary material available at https://doi.org/10.1038/s41528-025-00415-6.

Correspondence and requests for materials should be addressed to Bo-Yeon Lee or Sin-Hyung Lee.